ULTRASONIC IMAGING **25**, 73-84 (2003)

Improved Fourier-Transform-Based Parallel Receive Beam Formation

MENG-LIN LI AND PAI-CHI LI

Department of Electrical Engineering
National Taiwan University
Taipei, Taiwan
paichi@cc.ee.ntu.edu.tw

A Fourier transform (FT)-based technique for forming parallel receive beams has been previously employed to increase the imaging frame rate in ultrasonic imaging. However, the image quality in FT-based parallel reconstruction is degraded because differences in range focusing delays are ignored and a wide transmit beam needs to be used. In this paper, an adaptive weighting technique based on a focusing-quality index is used to reduce the sidelobes of the FT-derived parallel receive beams. The focusing-quality index is derived from the spatial spectrum of the received aperture data after the receive delays have been applied. Since the spatial spectrum of the baseband aperture data is also used to approximate receive beams in FT-based parallel reconstruction, the adaptive weighting technique can be directly combined with the FT-based technique for forming parallel receive beams with only a slight increase in system complexity. Real ultrasound data are used to demonstrate the efficacy of the proposed technique on both wire targets and speckle-generating objects. The results clearly demonstrate the effectiveness in reducing the sidelobes. In addition, the image background noise is suppressed. The principles, experimental results, and the extension of the proposed technique to 3D ultrasound imaging are described in this paper.

KEY WORDS: Focusing-quality index; parallel receive beam formation; 3D ultrasound imaging.

I. INTRODUCTION

In conventional ultrasonic imaging systems, the receive beams are formed sequentially, with one receive beam along the transmit direction being formed after one transmit burst. Therefore, the sound velocity in the tissue fundamentally limits the data acquisition rate of such systems. A higher data acquisition rate makes it is possible to acquire more images (within a given time interval) that can be compounded to reduce speckle noise, or to reduce the average radiation exposure to the patient while maintaining the same display frame rate.[1] Other potential applications requiring high frame rates include cardiac imaging, color flow imaging and real-time 3D imaging. The data acquisition time particularly limits the frame rate in real-time 3D imaging.[2, 3]

To obtain a higher data acquisition rate, several techniques for forming multiple receive beams have been proposed.[1, 4–7] These techniques simultaneously produce multiple receive beams along different directions so that the data acquisition rate is increased by a factor equal to the number of reconstructed receive beams per transmit event. Each receive beam has its own reception time delays, and the respective time delays are applied to the same channel data prior to individual beam summation. The pulse-echo beam pattern for each beam produced in this manner is the product of the transmit beam pattern and the corresponding receive beam pattern. Hence, only receive beams close to the center of the transmit beam can be effectively synthesized.[1]

Reconstructing multiple receive beams requires parallel processing, which increases the system complexity. Conceptually, a duplicate beam former is needed for each simulta-

0161-7346/03 $18.00

neously received beam. Practically, several methods have been proposed to reduce the system complexity associated with parallel processing. Shattuck et al. used the delay similarity on each channel between adjacent receive beams to propose a parallel processing approach for a phased array sector scanner, named "Explososcan."[1] In Explososcan, small tapped delay lines added at each receive channel after the main delay system replaced a completely independent beam former for each additional receive beam. In their study, four simultaneous receive beams were formed for each transmit beam. The transmit beam needs to be sufficiently broad such that all the receive beams acquire data from all directions with sufficient insonification. A time multiplexing scheme has also been proposed for the formation of parallel receive beams.[6] Using two beams as an example, the sampled receive data are time multiplexed, in which the odd-number samples are used to form one beam and the even-number samples are used to form the other beam. Formation of the two receive beams is switched in time. The formation of three or four parallel beams can be implemented in a similar fashion. With time multiplexing, the hardware complexity is reduced but the reduced clock rate produces a lower system bandwidth that may affect the axial resolution.

Alternatively, the parallel processing of received beams can be greatly simplified by ignoring the small time delay difference for neighboring beams on a given channel. Using the parabolic approximation, the time delay for a given array element is the sum of a range focusing term and a steering term. When the range focusing term is ignored, the formation of parallel beams can be approximated by Fourier transforming the baseband aperture data (i.e., the received channel data along the array direction). Based on this property, O'Donnell developed an efficient technique for forming parallel receive beams in phased array imaging.[7, 8] Two receive beams were formed with only a slight increase in hardware complexity. However, ignoring the focusing delay difference among different receive beams degrades the quality of the receive beams.

This paper introduces an adaptive weighting technique that was previously developed to reduce the focusing errors resulting from sound-velocity inhomogeneities.[9, 10] The adaptive weighting technique is extended to Fourier transform (FT)-based formation of the parallel receive beams. The adaptive weighting is based on a focusing-quality index, known as the generalized coherence factor (GCF).[9, 10] The GCF is derived from the spatial spectrum of the received aperture data after the receive delays have been applied. In this study, the GCF is employed to reduce the sidelobes of the FT-derived parallel receive beams. Since the spatial spectrum of the aperture data is used to approximate parallel receive beams, the GCF weighting technique can be directly combined with FT-based formation of parallel beams with only a small increase in system complexity. In this paper, real ultrasound data are used to evaluate the efficacy of the proposed technique on both wire targets and diffuse scatterers. The effects on contrast resolution and background noise level are explored. The extension of the proposed technique to 3D ultrasound imaging is also discussed.

The paper is organized as follows. In section II, FT-based formation of parallel receive beams is first reviewed. The adaptive weighting technique based on the GCF is introduced and extended to FT-based parallel reconstruction in section III. In section IV, real ultrasound data are used to evaluate the performance of the adaptive weighting technique, concentrating on sidelobe reduction in images. The paper concludes in section V.

II. FT-BASED PARALLEL RECONSTRUCTION

The channel data are defined as the data received by each array channel after the focusing delays of a particular receive direction are applied prior to beam summation. At a particular range, the data received by each channel i across the array is also called the aperture data and is denoted as $S(i)$. The time index is fixed at a particular range and thus is omitted in the above notation. Parallel receive beams can be simultaneously reconstructed using the FT of the baseband aperture data. The discrete Fourier spectrum across the array can be viewed as the approximation of multiple parallel receive beams centered at a prespecified direction (it is typically the transmit direction) and equally spaced by

$$\sin\theta = \lambda/(Nd) \tag{1}$$

where θ is the steering angle in a sector scan, d is the pitch of the array, λ is the wavelength, and N is the number of points in the discrete spectrum.[7,8] Note that N determines the spacing of the reconstructed beams.

The N-point discrete Fourier spectrum of the aperture data can be expressed as

$$p(k) = \sum_{i=0}^{N-1} S(i) e^{-j2\pi(id)\frac{k}{Nd}} = \sum_{i=0}^{N-1} S(i) e^{-j2\pi\frac{ik}{N}} \tag{2}$$

where $k = -N/2$ to $N/2-1$ is the spatial frequency index, which can also be used as the receive beam index. If the length of $S(i)$ is less than N, $S(i)$ is zero padded to length N. The discrete Fourier transform can be efficiently computed using the fast FT (FFT). Note that the negative and positive parts of k represent equally spaced beam directions on each side of the center of all receive beams (i.e., $k = 0$). In other words, the dc component (i.e., $p(0)$) represents the received signal from the prespecified primary receive direction and the high-frequency components correspond to the approximated receive beams from other angles.

In practice, only the receive beams near the center of the transmit beam can be effectively synthesized. Hence, the transmit beam should be broadened for the formation of parallel receive beams and the transmit beam spacing is equal to the one-way Nyquist beam spacing $\lambda/N_t d$, where N_t is the number of transmit channels. Note that the transmit beam width can be adjusted by varying N_t. The geometry of n parallel receive beams using the FT approximation is illustrated in figure 1 with $n = 3$ (i.e., three beams). In this case, three beams are received within the transmit beam. The thick solid arrow represents the center receive beam direction and the two dotted arrows are the additional parallel receive beams. The region within the two dashed lines in figure 1 is defined as the effective region for the i-th transmit beam (Tx_i). The n parallel receive beams are evenly spaced by $\lambda/(nN_t d)$. Comparing this spacing with that defined in Eq. (1), the number of points in the discrete spectrum is equal to n times the number of transmit channels, i.e.,

$$N = nN_t \tag{3}$$

In addition, the spacing of the n parallel receive beams needs to satisfy the two-way Nyquist criterion, with the two-way effective aperture size being $(N_t+N_r)d$. In other words, N_t and N_r must be chosen such that $\lambda/(nN_t d) \le \lambda/[(N_t+N_r)d]$.[11] Thus, the number of transmit channels used in FT-based parallel reconstruction can be expressed as

$$N_t \ge \frac{N_r}{n-1}, \tag{4}$$

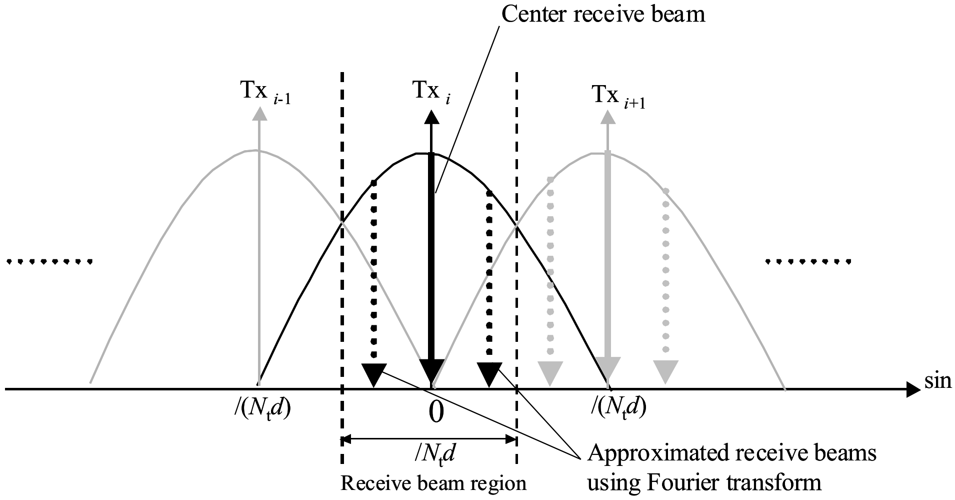

FIG. 1 Illustration of the geometry of three parallel receive beams. The thick solid arrow indicates the center receive beam direction and the two dotted arrows are the parallel receive beams with approximated delays.

where is the ceiling function (i.e., the smallest integer that is larger than the value of the input parameter). Given the number of receive channels and the number of parallel receive beams for each transmit event, the number of transmit channels is first calculated using Eq. (4). Then, the number of points used in the FFT can be determined based on the receive beam spacing and Eqs. (3) and (4) to satisfy the two-way Nyquist beam sampling criterion. Although the FT-based technique for forming parallel receive beams can efficiently reconstruct parallel receive beams, focusing errors are introduced since the focusing delay differences are ignored. Such focusing errors, as well as the need for a wider transmit beam, limit the performance of the FT-based technique for forming parallel receive beams and need to be corrected.

III. ADAPTIVE WEIGHTING TECHNIQUE

In this section, an adaptive weighting technique previously proposed for phase aberration correction is extended and combined with the FT-based technique for forming parallel receive beams. The weighting factor (i.e., the GCF) is derived from the spectrum of the aperture data after appropriate receive delays have been applied prior to beam summation and after baseband demodulation. The GCF is an index of the focusing quality, where a high GCF corresponds to good focusing quality and thus the image intensity is maintained. A low GCF, on the other hand, should be used to reduce the image intensity since significant focusing errors are present.[9, 10] Ignoring the range focusing delay differences in FT-based parallel reconstruction makes the focusing imperfect – GCF adaptive weighting can be employed to reduce such imperfection and to further lower the sidelobes of the FT-derived parallel receive beams. In addition, since the spatial spectrum of the aperture data used to derive the GCF is readily available for FT-based formation of parallel receive beams, the GCF weighting technique can be directly combined with FT-based parallel reconstruction with only a small increase in system complexity.

For the formation of parallel receive beams, the GCF is defined as the ratio of the energy received from angles near the reconstructed receive beam direction to the total energy from all directions. Based on the relationship between parallel receive beams and the Fourier

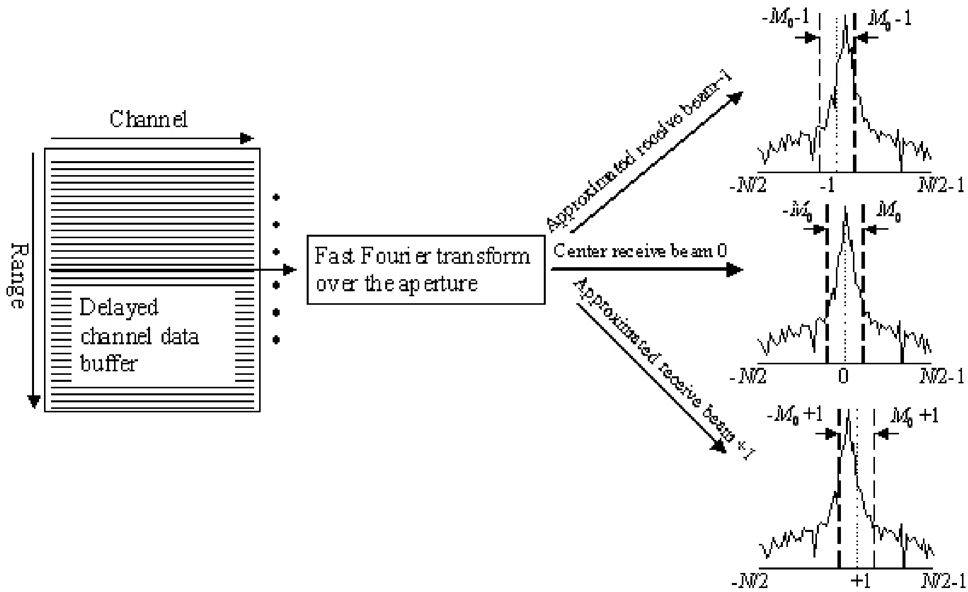

FIG. 2 Schematic diagram showing how the GCF for three beams is calculated.

spectrum over the aperture data, as described in section II, the GCF can also be viewed as the ratio of the spectral energy within a prespecified frequency range centered at the spatial frequency representing the reconstructed receive beam direction to the total energy. Hence, for FT-based parallel reconstruction, the GCF for one reconstructed receive beam l at a given range can be expressed as

$$\mathrm{GCF}_l = \frac{\sum_{k=-M_0+l}^{M_0+l} |p(k)|^2}{\sum_{k=-N/2}^{N/2-1} |p(k)|^2} \tag{5}$$

where M_0 is a cutoff frequency specifying the frequency range in the spatial frequency index (i.e., from $-M_0$ to M_0). For three receive beams, the reconstructed receive beam index l ranges from -1 to 1: $l = 0$ represents the center receive beam, and $l = -1$ and 1 indicate respectively the left and right approximated receive beams as indicated by the two dotted arrows in figure 1. The procedure for calculating the GCF for three beams is illustrated in figure 2. Note that while imaging a speckle-generating target, the cutoff frequency M_0 cannot be restricted to zero since it needs to be large enough to include the inherent incoherence of such a target.

As described above, the image quality of FT-based parallel reconstruction can be improved via GCF weighting. The GCF-weighted signal $x_{l\text{-weighted}}$ of x_l for the receive beam l at a given range can be expressed as

$$x_{l\text{-weighted}} = \mathrm{GCF}_l \times x_l \tag{6}$$

Note that for each receive beam, the weighting needs to be calculated and applied at each imaging depth. Figure 3 shows the system block diagram of the GCF technique for three

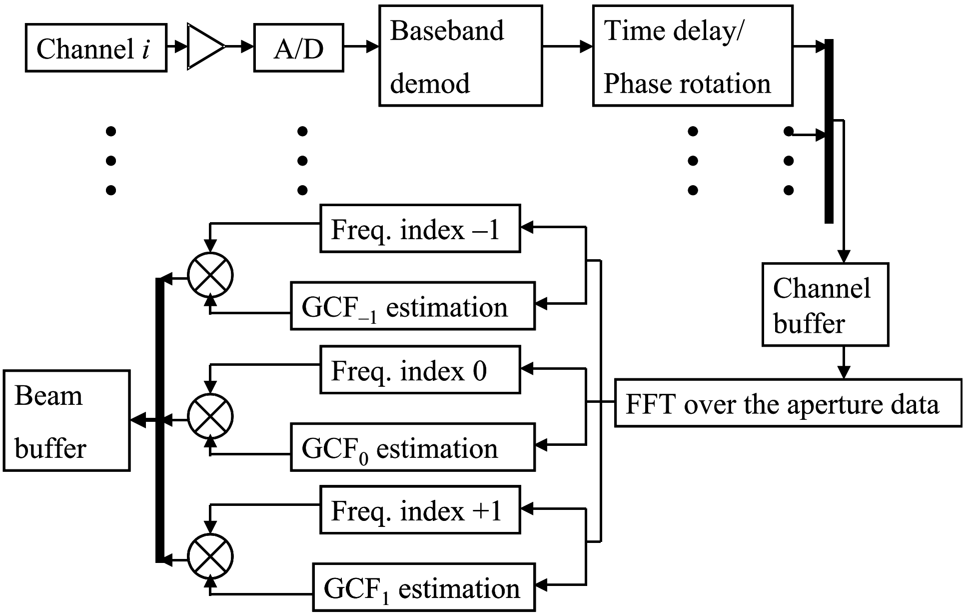

FIG. 3 System block diagram of the adaptive weighting technique for three beams.

beams. The echo signal for one transmit event is received and digitized by an analog-to-digital converter, and then the received rf data are demodulated down to baseband. The baseband beam former applies the correct dynamic receive delays and phase rotations along the center receive direction (as indicated by the solid arrow in figure 1) before the data are sent to the channel buffer. The parallel receive beams and their corresponding GCFs are then estimated using the FFT of the delayed baseband array data (note that the GCFs need to be calculated at all range points). The spectral components at frequency indices of –1, 0, and 1 (i.e., the three beams illustrated in figure 1) are then weighted by the corresponding GCFs based on Eq. (6) on a point-by-point basis. The weighted data are then sent to the beam buffer for further signal processing, scan conversion and display. Note that the reconstructed receive beams and their corresponding GCFs can be efficiently computed via the FFT at the same time. As illustrated in figure 3, the proposed GCF technique can be easily incorporated into the FT-based technique for forming parallel receive beams.

IV. EXPERIMENTAL RESULTS

In this section, simulated images using real ultrasound data are presented to evaluate the efficacy of the proposed technique. All the raw data files are available from http://bul.eecs.umich.edu. They were acquired using a 128-element, 3.5 MHz phased-array transducer (Acuson V328, Mountain View, California, USA) at a 13.8889 MHz sampling rate. Data from a wire phantom and a tissue-mimicking phantom were used. The wire phantom consisted of six nylon wires in water, arranged at ranges of 34, 48, 65, 83, 101 and 121 mm. For all images, the transmit focus was 60 mm from the transducer and dynamic receive focusing with an f-number of 1.5 was applied. Here, three receive beams were reconstructed. Since the entire array transducer (i.e., 128 channels) was used on receive, according to Eqs. (3) and (4), the middle 64 channels were used on transmit, and a 192-point FFT was applied for parallel reconstruction. Cutoff frequencies of $M_0 = 2$ and $M_0 = 8$ were used for the wire

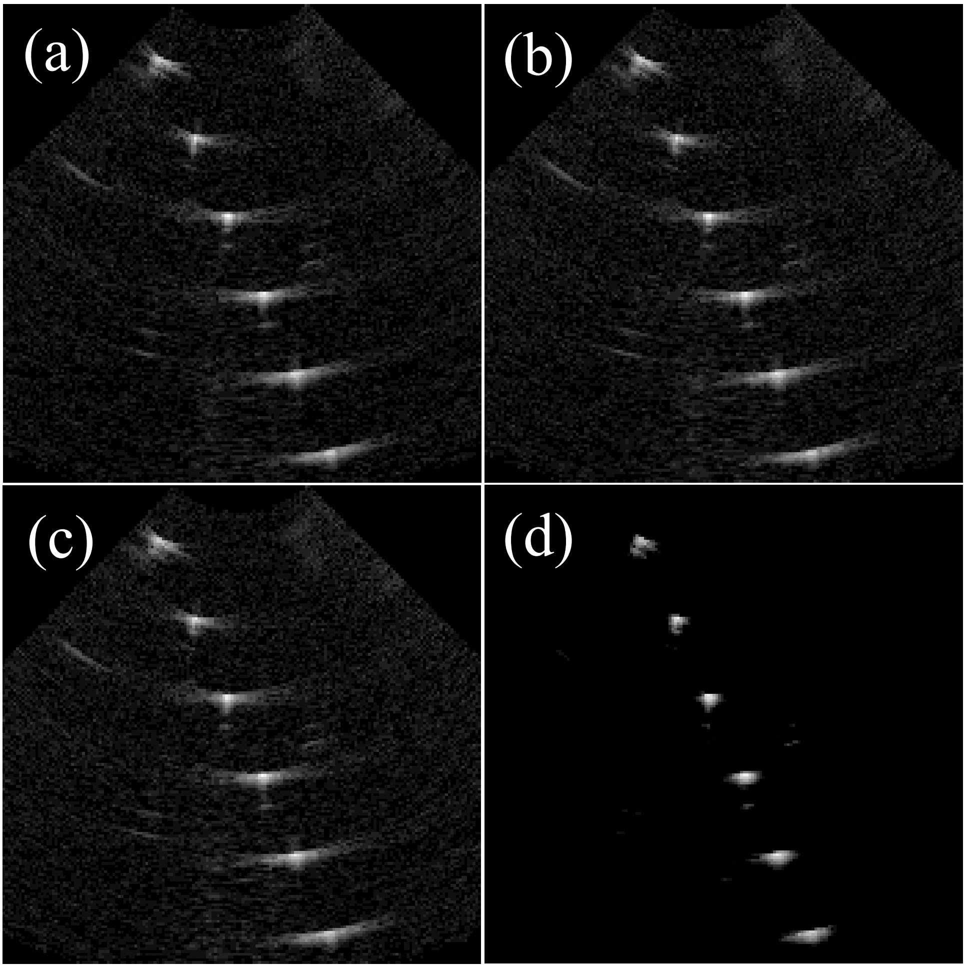

FIG. 4 Images of a six-wire phantom, displayed with an 80-dB dynamic range. The vertical axis is the depth and the horizontal axis is the lateral distance. (a) is the image with standard scanning. (b) is the three-beam image assuming duplicate beam formers. (c) and (d) are the three-beam images of FT-based parallel reconstruction without and with GCF weighting, respectively.

phantom and the tissue-mimicking phantom, respectively. In addition, since the receive beams are along different directions relative to the center of the transmit beam, the resulting variations among the parallel receive beams result in asymmetry in the two-way beam pattern. For the formation of n parallel receive beams, this causes periodic variations of the image intensity (with a period equal to n). The variations are more pronounced when the steering angle is larger. Hence, an n-tap moving-average filter (i.e., with filter coefficients of $[1/n \ 1/n \ ..1/n]$) needs to be applied laterally to smooth out these artifacts. All images are shown here in the format after scan conversion (i.e., the horizontal axis is the lateral distance in millimeters and the vertical axis is the depth away from the transducer in millimeters).

A. Wire phantom

Figure 4 shows the images for the wire phantom, displayed with an 80-dB dynamic range. Figure 4(a) is the image with standard scanning (i.e., one receive beam along the transmit direction for each transmit event). Figure 4(b) is the three-beam image assuming duplicate

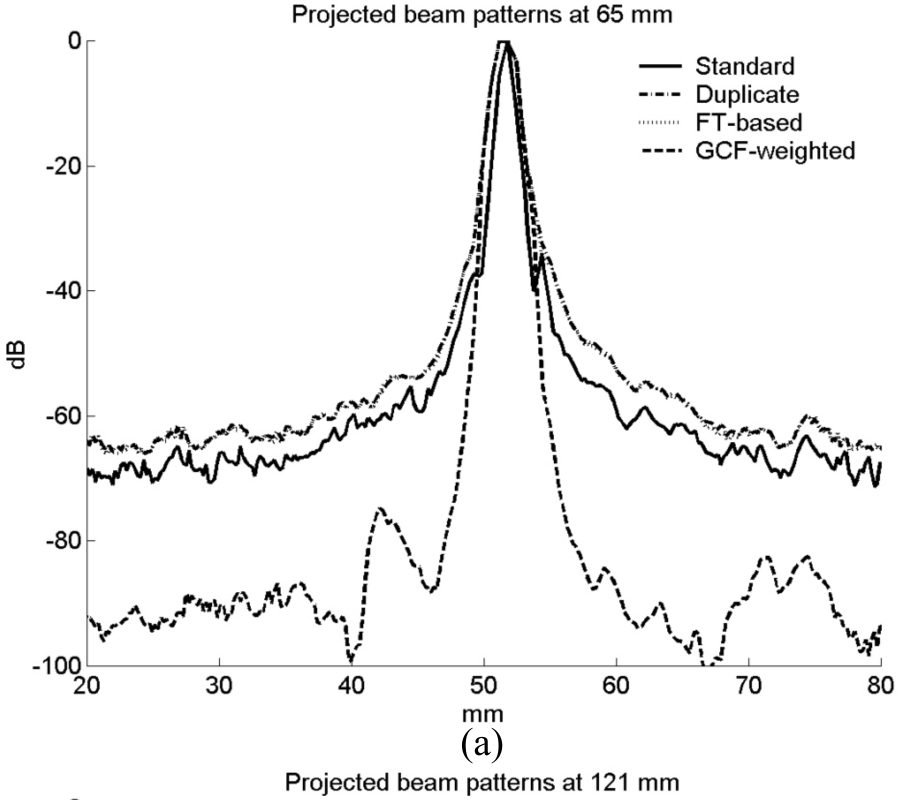

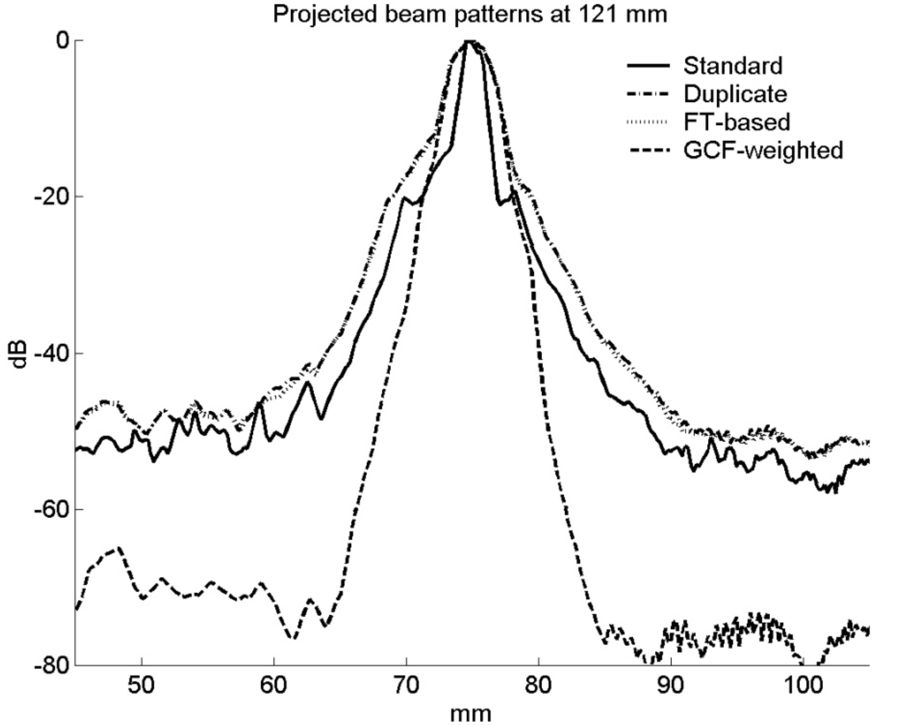

FIG. 5 Projected radiation patterns of the two wires at 65 mm (a) and 121 mm (b) in figure 4. The solid lines are the case with standard scanning. The dotted–dashed line is the three-beam case assuming duplicate beam formers. The dotted and dashed lines are the three-beam cases using FT-based parallel reconstruction before and after adaptive weighting, respectively.

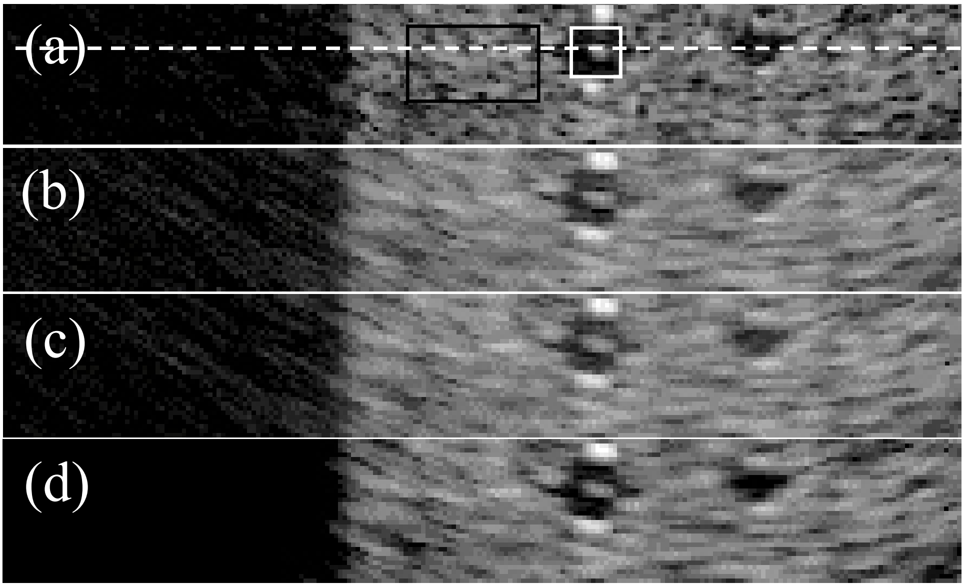

FIG. 6 Images of a tissue-mimicking phantom with anechoic cysts, displayed with a 40-dB dynamic range. The vertical axis is the depth and the horizontal axis is the lateral distance. (a) is the image with standard scanning. (b) is the three-beam image assuming duplicate beam formers. (c) and (d) are the three-beam images of FT-based parallel reconstruction without and with GCF weighting, respectively. The black and white boxes indicate the background and cyst regions used for CNR calculations, respectively.

beam formers (i.e., three receive beams are reconstructed simultaneously by applying their corresponding time delays to the same channel data). Figures 4(c) and 4(d) are the three-beam images using FT-based parallel reconstruction before and after GCF weighting, respectively. The channel counts on transmit and receive for the four cases are the same. The width of the four images is 110 mm and the depth ranges from 21.79 mm to 131.79 mm. Note that the two parallel-reconstructed images (figures 4(b) and 4(c)) look similar, but the signal-to-noise ratio (SNR) is lower than in the image with standard scanning (figure 4(a)). Comparison of figures 4(c) and 4(d) reveals that both the sidelobe level and image background noise are noticeably suppressed by the adaptive weighting technique.

Figures 5(a) and 5(b) show the projected beam patterns of the wires at 65 and 121 mm, respectively, of the images in figure 4. For both wires, note that the beam patterns of both parallel-reconstructed images have wider mainlobes than those with standard scanning. The moving-average filter widens the mainlobe and hence degrades the lateral resolution, although this also can reduce the image-intensity variations resulting from the transmit beam asymmetry. The beam pattern of FT-based parallel reconstruction has higher sidelobes and noise level than that with standard scanning. The sidelobe level of the FT-based parallel-reconstructed image is suppressed by about 10 dB after weighting. In addition, the noise floor of the weighted image is about 20 dB lower than that of the unweighted image when using FT-based parallel reconstruction.

B. Tissue-mimicking phantom

Data from a tissue-mimicking phantom (RMI-412R, Gammex RMI, Middleton, Wisconsin, USA) with anechoic cysts were also used to evaluate the efficacy of the adaptive weighting technique in improving contrast resolution. Images (with a 40-dB dynamic range) in the vicinity of a cyst at 72 mm are shown in figure 6. Figures 6(a)–(d) are the images with stan-

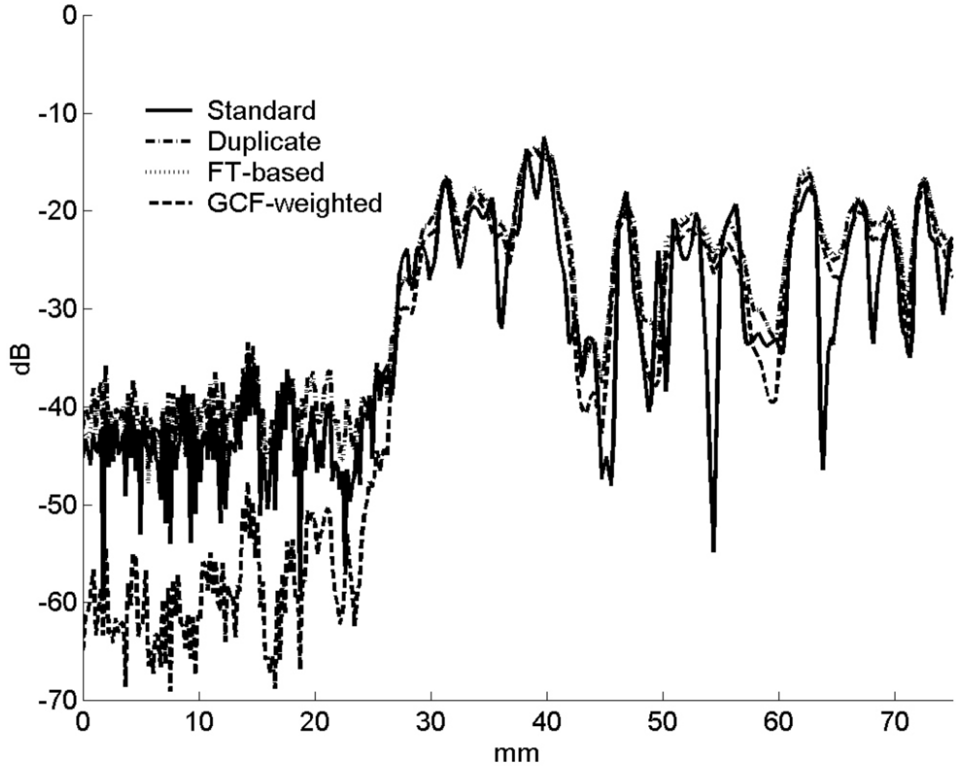

FIG. 7 The image intensity of the four images in figure 6 along the horizontal white dashed line shown in figure 6(a).

dard scanning, duplicate beam formers, FT-based parallel reconstruction and GCF weighting, respectively. The width of the four images is 75.20 mm; the depth ranges from 68.42 mm to 79.16 mm. Figure 6 shows that GCF weighting improves the image quality of FT-based parallel reconstruction. The cyst detection is noticeably improved after adaptive weighting in that the weighted image is less 'filled in' in the cyst region than the image using FT-based parallel reconstruction without weighting. The weighted image also exhibits superior edge definition and sharper contrast. Again, the image background noise is suppressed by adaptive weighting. Figure 7 shows the image intensity along the horizontal white dashed line shown in figure 6(a). In addition to sidelobe reduction, GCF weighting reduces the noise floor in the left portion of the image by about 20 dB.

The contrast-to-noise ratio (CNR) is employed to quantitatively evaluate the improvement in contrast resolution. The CNR is calculated by taking the ratio of the image contrast to the standard deviation of image intensity in the background region, where the contrast is defined as the difference (in decibels) between mean intensity values in the background and in the cyst region.[8] The background and cyst regions are indicated respectively by the black and white boxes in figure 6(a). The CNRs are 1.98 for the standard-scan image, 2.29 for the parallel-reconstructed image with duplicate beam formers, 2.33 for the FT-based parallel-reconstructed image and 2.64 for the GCF-weighted image. Because the moving-average filter reduces speckle noise, the CNR in the two parallel-reconstructed images (figures 6(b) and 6(c)) is higher than that with normal scanning. Nonetheless, the CNR is further increased after weighting. It is demonstrated that adaptive weighting can effectively improve the image quality of FT-based parallel reconstruction by reducing the sidelobes.

V. CONCLUDING REMARKS

The adaptive weighting technique using the GCF was previously developed to reduce the focusing errors resulting from sound-velocity inhomogeneities. In this paper, this technique has been extended to improve the degraded beam quality of the FT-based technique for forming parallel receive beams. Experimental results from a wire phantom and a tissue-mimicking phantom demonstrate the effectiveness of the adaptive weighting technique: the sidelobe level was effectively suppressed and contrast resolution was noticeably improved. The image background noise was also lower after applying the weighting. Due to the relationship between parallel receive beams and the Fourier spectrum over the aperture data, this weighting technique can be implemented efficiently. The proposed GCF technique can be incorporated into FT-based parallel reception systems with only minor modifications.

The GCF in Eq. (5) is defined without taking noise into consideration. The relationship between GCF without noise (i.e., an infinite SNR) and the estimated GCF with a finite SNR (denoted by GCF') has been discussed previously.[10] If the SNR is much less than unity, the estimated GCF can be expressed as

$$\mathrm{GCF}' \approx \frac{(2M_0 + 1)}{N} \tag{7}$$

In our case, given $M_0 = 8$ and $N = 192$, the estimated GCF is about 0.09. Since the SNR in the image background (i.e., the anechoic region) is very low, applying such weighting reduces the image intensity. Thus, as shown in section IV, the adaptive weighting technique effectively suppresses the noise floor in the image background. In addition, a simple moving-average low-pass filter is used to smooth out the image-intensity variations resulting from beam asymmetry in this paper. However, such a simple filter reduces the spatial resolution in all types of parallel beam forming techniques.

The proposed GCF weighting technique can be directly extended to improving the quality of real-time 3D imaging using 2D arrays. For 3D imaging using 2D arrays, the GCF of one reconstructed receive beam (l, m) can be defined as follows:

$$\mathrm{GCF}_{l,m} = \frac{\sum_{k_x=-M_{x0}+l}^{M_{x0}+l} \sum_{k_y=-M_{y0}+m}^{M_{y0}+m} \left|p(k_x,k_y)\right|^2}{\sum_{k_x=-N_x/2}^{N_x/2-1} \sum_{k_y=-N_y/2}^{N_y/2-1} \left|p(k_x,k_y)\right|^2} \tag{8}$$

where $p(k_x,k_y)$ is the 2D Fourier spectrum over the 2D aperture data with N_x points in the lateral direction and N_y points in the elevational direction, k_x and k_y are the 2D spatial indices along the lateral and elevational directions of the 2D array, respectively, and M_{x0} and M_{y0} are the cutoff frequencies specifying the frequency range in the spatial frequency domain (i.e., from $-M_{x0}$ to M_{x0} and from $-M_{y0}$ to M_{y0}). Although the results demonstrated here are only for 2D imaging using 1D arrays, it is expected that the proposed weighting technique can produce similar improvements to 3D imaging with the FT-based technique for forming parallel receive beams using 2D arrays.

ACKNOWLEDGMENT

Data used in this paper was downloaded from the Biomedical Ultrasonics Laboratory at the University of Michigan (http://bul.eecs.umich.edu).

REFERENCES

1. Shattuck, DP, Weinshenker, MD, Smith, SW, von Ramm, OT. Explososcan: a parallel processing technique for high speed ultrasound imaging with linear phased arrays, *J Acoust Soc Am 75,* 1273–1282 (1984).

2. Smith, SW, Pavy Jr, HG, von Ramm, OT. High-speed ultrasound volumetric imaging system – Part I: transducer design and beam steering, *IEEE Trans Ultrason Ferroelect Freq Contr 38,* 100–108 (1991).

3. von Ramm, OT, Smith, SW, Pavy Jr, HG. High-speed ultrasound volumetric imaging system – Part II: parallel processing and image display, *IEEE Trans Ultrason Ferroelect Freq Contr 38,* 109–115 (1991).

4. Delannoy, B, Torguet, R, Bruneel, C, Bridoux, E, Rouvaen, JM, LaSota, H. Acoustical image reconstruction in parallel-processing analog electronics systems, *J Appl Phys 50,* 3153–3159 (1979)

5. Koyano, A, Yoshikawa, Y, Konishi, et al. A high quality ultrasound imaging system using linear array transducer, *Ultrasound Med Biol 8,* 100 (1982).

6. Gee, A, Cole, CR, Wright, JN. Method and apparatus for focus control of transmit and receive beamformer systems, *U.S. Patent 5,581,517* (1996).

7. O'Donnell, M. Efficient parallel receive beam forming for phased array imaging using phase rotation, in *Proc IEEE Ultrason Symp,* pp. 1495–1498 (1990).

8. Krishnan, S, Rigby, KW, O'Donnell, M. Efficient parallel adaptive aberration correction, *IEEE Trans Ultrason Ferroelect Freq Contr 45,* 691–703 (1998).

9. Li, ML, Li, PC. A new adaptive imaging technique using generalized coherence factor, in *Proc IEEE Ultrason Symp* (2002).

10. Li, PC, Li, ML. Adaptive imaging using the generalized coherence factor, *IEEE Trans Ultrason Ferroelect Freq Contr 50,* 128–141 (2003).

11. Ucar, FN, Karaman, M. Beam spacing processing for low-cost scanners, in *Proc IEEE Ultrason. Symp,* pp. 1349–1352 (1996).